Visualization-Guided Evaluation of Simulated Minimally Invasive Cancer Treatment

P. Voglreiter[1], M. Hofmann[1], C. Ebner[1], R. Blanco Sequeiros[2], H.R. Portugaller[3],
J. Fütterer[4], M. Moche[5], M. Steinberger[6], and D. Schmalstieg[1]
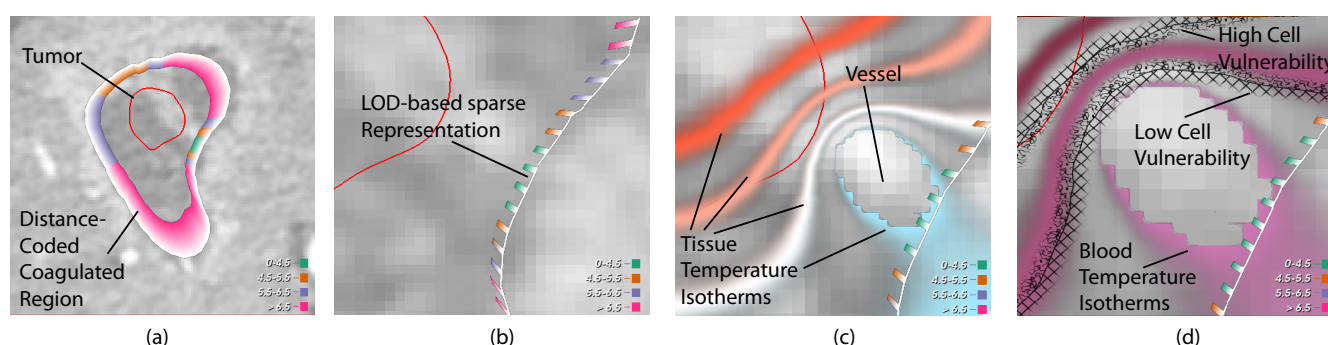
[1]Graz University of Technology, Austria
[2]Turku University Hospital, Finland
[3]University Clinic of Radiology Graz, Austria
[4]Radboud University Nijmegen Medical Center, Netherlands
[5]Leipzig University Hospital, Germany
[6]Max Planck Institute for Informatics, Saarbrücken, Germany

Figure 1: *A typical use-case of our visual analysis technique for evaluating simulations of minimally invasive cancer treatment. An interventional radiologist evaluates the safety margin of dead tissue around a tumor after simulated treatment (a) and encounters critical areas (orange and blue segments). Zooming in (b) unveils underlying patient data via a levels of detail-based approach and reveals a potential vessel (bright area). The radiologist decides to include the tissue temperature field from simulation via iso-contours (c) to further examine the finding. For final decision, the radiologist then analyses the dependence of blood temperature and tissue vulnerability (d). We provide a categorized, texture-based iso-contour representation, in this case categorizing into low and high values. After the radiologist identifies the cause of the issue, she updates the simulation parameters accordingly and tries to destroy the problematic vessel.*

Abstract

We present a visualization application supporting interventional radiologists during analysis of simulated minimally invasive cancer treatment. The current clinical practice employs only rudimentary, manual measurement tools. Our system provides visual support throughout three evaluation stages, starting with determining prospective treatment success of the simulation parameterization. In case of insufficiencies, Stage 2 includes a simulation scalar field for determining a new configuration of the simulation. For complex cases, where Stage 2 does not lead to a decisive strategy, Stage 3 reinforces analysis of interdependencies of scalar fields via bivariate visualization. Our system is designed to be immediate applicable in medical practice. We analyze the design space of potentially useful visualization techniques and appraise their effectiveness in the context of our design goals. Furthermore, we present a user study, which reveals the disadvantages of manual analysis in the measurement stage of evaluation and highlight the demand for computer-support through our system.

Categories and Subject Descriptors (according to ACM CCS): I.3.3 [Computer Graphics]: Picture/Image Generation—Line and curve generation

1. Introduction

Over the past years, minimally invasive cancer treatment (MICT) aspired as important therapy for patients disqualifying for classical surgical removal of tumors. Many of these methods locally destroy cancerous cells via inducing energy by coagulating tissue in the focused zone. An Interventional Radiologist (IR) percutaneously places a probe, connected to a generator, near the tumor. The choice of parameters drastically influences volume and shape of the coagulated area. Concerning treatment success, Nishikawa *et al.* [NIT*11] state that a safety margin of dead tissue around the tumor is critical in avoiding recurrence. Consecutively, only ideal planning, configuration and execution of these complex methods minimizes the risk of local tumor recurrence. Nevertheless, the current clinical routine almost exclusively relies on the experience of the IR.

However, predicting the outcome of such methods in advance received increased interest from the medical community over the last years. Unfortunately, most of the presented systems focus on the generation of simulated results and neglect the analysis stage required for pre-interventional optimization of the treatment parameters. We present a visualization system tailored towards the needs of the clinical routine for both speeding up the analysis of predicted coagulation regions and indirectly aiding the IR in adapting parameters for iteratively improving the parameterization.

1.1. Pre-Interventional Simulation

Recent advances in bio-mechanical simulation show that high-accuracy, patient-specific prediction of MICT can be achieved faster than real-time [BHA14] [AMD*15]. This allows the IR to prospectively explore the parameter space and iteratively improve the configuration until achieving a satisfying result for conservative treatment. They can minimize the risk for local tumor recurrence in advance by finding a configuration which satisfies the required safety margin, while at the same time spares as much healthy tissue as possible.

1.2. Evaluation Procedure

We break down the evaluation of simulated MICT into three steps. In Stage 1, the IR needs to evaluate whether the predicted coagulated region sufficiently covers the tumor and includes the required safety margin. If the prospective result is unsatisfactory, Stage 2 requires analysis of the reasons for failure. For example, the distribution of energy near the tumor can reveal potentially critical regions. Such information can already reveal a clear way to modify the parameterization, but occasionally, deeper understanding of a case is required. Therefor, the Stage 3 concentrates on the interdependency of contributing factors. For example, tissue perfusion considerably influences the energy distribution in tissue [POP*10]. The gathered insight from these steps contributes to a new configuration for the simulation and, potentially, a more satisfying coverage.

However, only a handful of tools for aiding the IR in examining such predictions for reasoning on proper parameter adjustment exists. The current clinical routine only implements rudimentary tools, such as manual 2D measurement on simple outlines of the coagulated area and the tumors. These methods are not only tedious, but inherently prone to inaccuracies (see Figure 2(a)).

1.3. Contribution

We propose a system for fast and accurate evaluation of simulation results for energy-based MICT procedures. We provide techniques for incremental reasoning on the success of treatment and potential causes of insufficiencies from simulation data. Since such issues can arise from a broad range of parameters, our system is highly configurable. We formulated the following design goals for providing a toolset that fulfills the needs of an IR in their everyday environment:

- Applicability: The system needs to find wide acceptance among the user groups both in terms of visualization and interaction. Simplicity of setup and interpretation are key elements.
- Modularity: The application should provide a granular structure which enables modifying the level of detail (LOD) and number of variables presented to the user. Thereby, it supports multiple configuration levels, ranging from overview representation to detail analysis.
- Locality: Our visualization must retain the spatial reference points of data, *i.e.*, display data in the reference frame provided by the patient images.
- Clarity: The system must provide clear categorization of dense data fields, where necessary. The visual representation, however, should be sparse to avoid unnecessary obstruction of underlying patient data and undesired reciprocation of techniques.
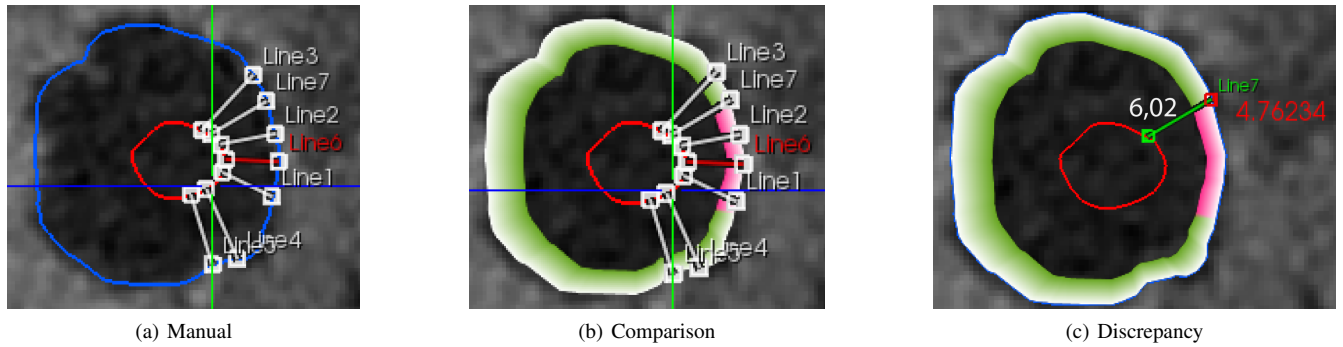
2. Related Work

Visual support for the whole process of evaluating prospective simulation of MICT is rarely discussed in previous work. Especially in the context of exploring the parameter space for incremental improvement of the prediction, related methods do not provide support for the full scope of tasks inherent to the procedure.

Closely related to our application, Rieder *et al.* [RWS*10] propose a method for visualizing the distance between a tumor and a coagulated area via surface unwrapping. The authors facilitate an external view for showing the distance to the coagulation zone via color coding on the unwrapped surface of the tumor. However, discussions with interventional radiologists revealed that they have a strong preference for data representation in their daily environment. Typical radiological workstations provide three views with planar, usually orthogonal slice reconstructions, whereas for abdominal images, the axial view is used most frequently.

Additionally, Rieder *et al.* [RKSH11] propose using iso lines for encoding the distance between coagulated area and tumor in combination with a semi-transparent overlay of the region comprising dead cells. They introduce a multi-parameter representation for displaying iso-distances over multiple time steps. In a related publication, Rieder *et al.* [RSW*09] display the cell death likelihood within the simulation domain using a fixed color scheme. However, both methods occupy an almost identical area on the patient image, making a combined visualization of multiple parameters difficult.

However, in our opinion, these methods do not provide sufficient modularity and locality and cannot easily be combined, so we propose a different approach.

| (a) Manual | (b) Comparison | (c) Discrepancy |

Figure 2: *Inaccurate manual measurement. (a) We show a measurement scenario on axial slices for evaluating the distance between the predicted coagulated region (blue) and the tumor (red). Only for Line 6, highlighted in red, the measured distance is shorter than the safety margin of 5 mm. (b) However, our method shows that the whole pink area between Line 1 (5.18mm) and Line 7 (6,02mm) is actually closer than 5 mm. (c) We computationally evaluate and display the distance at the end point of Line 7 (red text), revealing an error of more than 1.2 mm. The reasons for such inaccuracies results both from uncertainties in finding the shortest distance from the point on one surface to the second one, but also from the lack of 3D information. Even if the user measures the in-plane distance correctly, the actual 3D distance can still differ considerably.*

2.1. Distance Evaluation

Marshall and colleagues [MGT15] describe Proximity Map Projection, an unwrapping algorithm for evaluating spatial gaps and intersections of two surfaces. Such techniques ideally highlight the complex spatial relationships in an overview. However, the mental effort for relating the unwrapped view to the physical coordinate frame might be high, and the need for additional views does not agree with our goal of locality. Reitinger *et al.* [RSBB06] describe measurement tools for augmented reality-based surgery planning. Albeit such systems provide full 3D interaction, their applicability in the current clinical workflow is limited due to the overhead on hardware and training requirements. Preim and colleagues [PTSP02] discuss possibilities of visualizing 2D measurements, such as ruler-based distances and angles, in 3D. However, they do not provide advanced methods for improving the measurement process, which is a key aspect of our application. Dick *et al.* [DBW11] facilitate oriented glyphs in 3D for visualizing distances related to implant planning. They incorporate sparsely located slices in the 3D view for additional guidance. Pure 3D methods, however, find little acceptance amongst radiologists due to their strong preference for the higher precision of 2D slices. Moreover, the placement of the slices in the overview representation might lead to visual clutter in our application, even when considering only critical regions.

2.2. Multi-Field Simulation Visualization

Many approaches for visualizing multivariate data exist. For clarity, we split the related work into groups with similar metaphors. We then discuss their properties and suitability for our objectives.

Noise Various frequencies and representations of noise often find application in visualization. Botchen [BWE05], for example, compare noise injection with related techniques for visualizing uncertainty in dense flow fields. Similarly, Coninx *et al.* [CBDT11] map animated Perlin noise on visualizations generated by 1D color trans-

fer functions. Whereas such techniques work very well for making the user feel 'uncertain' about the displayed data, we doubt their applicability for our concept, since we emphasize on data evaluation with high confidence. Khlebnikov *et al.* [KKS*12] propose a zoom-independent application of random phase Gabor noise to multivariate visualization. In a user study, the authors show increased correctness and strong user preference of their method compared to previous approaches. However, visual categorization of data, which is one of our main goals, would be difficult due to the continuous characteristics of this visualization technique.

Glyphs Due to their expressiveness, glyphs are an established metaphor for multivariate visualization. Ropinski *et al.* [ROP11] summarize usage of glyph-based visualization techniques for medical purposes and provide general guidelines for using glyphs in encoding data. Since these approaches inherently discretize the data, optimal placement is a key element for perception. Ward [War02] presents a generalized taxonomy, whereas Kindlmann and Westin [KW06] propose a strategy for 'packing' glyphs for clearer representation.

However, our intentions differ from the typical use case of glyphs. Applications like diffusion tensor imaging of the brain benefit from encoding information such as flow orientation. The simulation of MICT, however, produces data of different nature. For example, the energy diffuses similar to a wavefront throughout the tissue. The cell death probability depends on energy absorption and is usually discontinuous and noisy. We do not think that glyph-based approaches positively impact the analysis of such data.

Multi-View Separability of visual variables naturally limits algorithms to simultaneous display of only a few data fields, raising the need for multiple views for analysis of additional dimensions. Roberts [Rob07] provides an overview of general structures employed for coordinated multiple views. For visualization of biomechanical motion data, Keefe *et al.* [KERC09] link 3D previews,

a parallel coordinate view for temporal data and a 2D plot of an additional variable. Since radiological workstations already employ multiple views for displaying several re-sliced views of patient data, adding even more views might increase the mental strain of evaluation. This is also the main reason why we formulated the design goal of locality, which such approaches clearly violate.

Texture A combination of color and texture often finds application in medical visualization. Multi-dimensional transfer functions [KHGR02] or direct combination of color and texture [UIM*03] [WFK*02] [HTER04] [SI05] are widely accepted techniques for multivariate visualization. The easy and quick interpretation of such approaches complies with our goal of clarity, while simple interaction techniques for setup of 2D transfer functions reinforces the applicability. Such setups also imply modularity, since one axis can be neglected, leading to a 1D transfer function. Finally, due to the direct application of visual parameters to the underlying data fields, we inherently achieve locality of the visualization.

3. Background

This section provides background on energy-based MICT simulation, both from a medical as well as a computational point of view. We first provide an overview of the medical workflow and considerations relevant for our application and follow up with a brief description of the parameter space involved in simulating shape and size of the coagulation zone.

3.1. Medical Background

All energy-based MICT procedures roughly follow the same workflow. Initially, in the pre-interventional phase, planning images from computed tomography (CT) or magnetic resonance imaging (MRI) serve for creating a patient model. This often includes contrast enhancement (CE) for better depiction of vessels and the tumor. Vessel trees significantly contribute to energy distribution due to the blood flowing through acting as temperature sink, whereas different kinds of tumors visualize differently on the CE phases. In some cases, patients additionally undergo perfusion measurement. All mentioned data contributes to a pre-interventional anatomical model for planning the parameterization of the upcoming intervention.

In the interventional phase, the IR performs the actual treatment. Patient motion, digestion and the current breathing phase significantly change the abdominal anatomy, requiring additional up-to-date patient images for accurate probe positioning. Once the IR is satisfied with the position, a suitable protocol is executed, which is usually chosen from one of several vendor-defined procedures. Depending on the size and shape of the tumor, several iterations with different protocols and probe positions may be necessary.

In the post-interventional phase, the IR monitors success over several years. Immediately after treatment, the boundary of the coagulated area does not visualize sufficiently due to bleeding and other post-interventional effects. General consensus names the depiction of the coagulation zone one month after treatment as final extent. Consequently, the IR cannot determine treatment success right after the intervention. Again, the clinical routine relies on the experience of the IR for deciding whether additional treatment is necessary.

3.2. Computational Background

The simulation procedure virtualizes the interventional phase. Initially, the IR virtually places the probe in either interventional or pre-interventional images. This additionally requires registration between pre-interventional and interventional images for reproducing the planned probe placement in the anatomical model. As in actual treatment, the IR chooses one or several consecutively executed protocols and generator parameterizations. The virtualization allows optimization of the parameters, including probe placement and generator configuration.

The simulation domain usually represents multiple data fields. The coagulation zone depends on the cell death probability, for which power emission and often temperature are critical. Biomechanical cell death models describe the dependency on time and the amount of deployed energy. Moreover, these factors usually interact with more complex parameters, such as specific heat capacity and perfusion of tissue. Patient-specific analysis of these dependencies may require multiple simulation iterations with adapted parameters until converging on a satisfactory result. However, as mentioned before, usual solutions offer little assistance for evaluating shortcomings in single configurations.

4. Method

In this section, we layout the modular structure of our approach and explain the evaluation procedure from overview to details. The analysis consists of three stages. Hence, we provide a visual metaphor for each subsequent step. Visualizations of the patient image and outlines of tumor and predicted coagulated region reflect the basic framework on which we build our advanced methods.

Completely failed treatment is comparatively easy to spot, since the outline of the coagulation zone does not fully enclose the tumor. Hence, we focus our considerations on cases which cover the tumor entirely, but the safety margin may be violated.
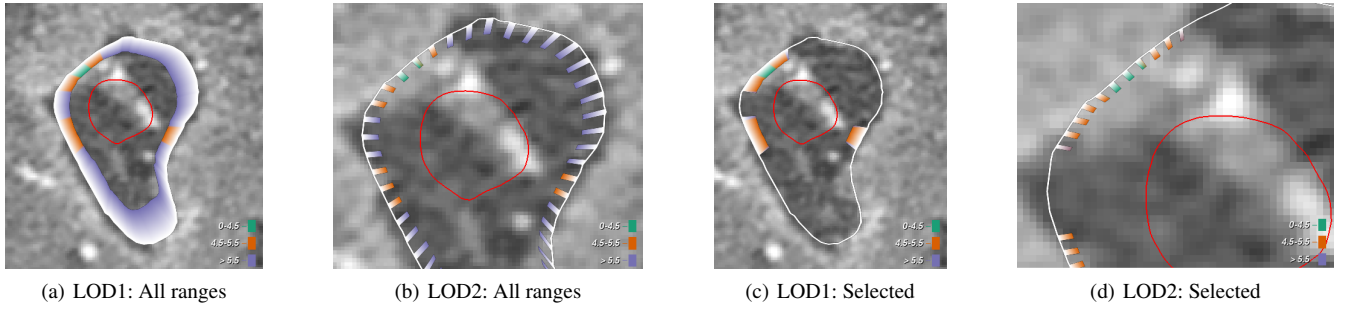
Stage 1: Initially, we aid the process of evaluating success of a simulation configuration by removing the need for manual measurements. As previously stated, MICT demands destroying the tumor plus a rim of healthy tissue around it. However, severe over-treatment, *i.e.*, coagulating large healthy portions of the organ, should be avoided. Therefore, we visualize the distance between simulated coagulation area and tumor in relation to the respective outlines.

Stage 2: In Stage 1, the user possibly identifies regions of the predicted coagulated region which do not satisfy the safety margin. In Stage 2, we additionally employ a customizable approach based on colored iso-contours for visualizing a single scalar field from the simulation.
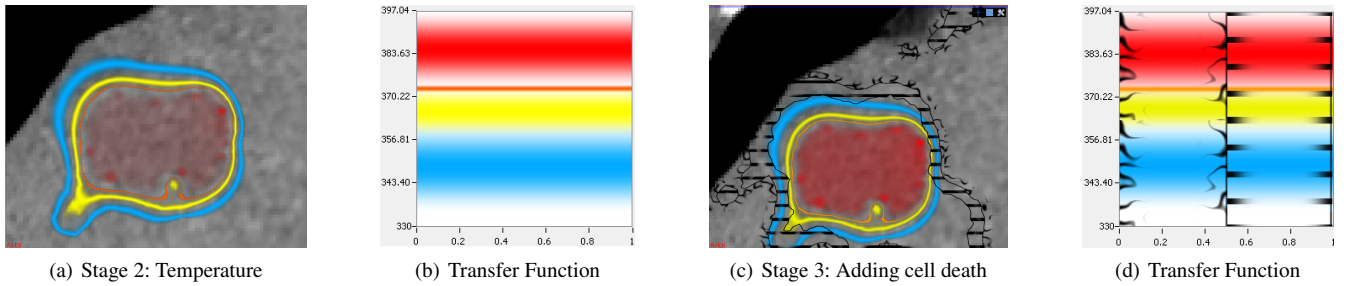
For example, emitted power or temperature are often informative during analysis of such failed regions. In combination with the Stage 1 visualization, the user can either immediately infer a new parameterization of the simulation or proceed with determining more complex interactions in Stage 3.

Stage 3: Parameter interdependencies often make the behavior of energy-based MICT hard to predict, and a single scalar field is often

(a) LOD1: All ranges   (b) LOD2: All ranges   (c) LOD1: Selected   (d) LOD2: Selected

Figure 3: *Several Settings for the distance visualization. (a) We display the 3D distance in a color-coded rim. When zooming in closer, the algorithm switches to a new LOD (b). The user can toggle the display of single ranges and only receive the currently relevant information in both levels of detail (c, d).*

(a) Stage 2: Temperature   (b) Transfer Function   (c) Stage 3: Adding cell death   (d) Transfer Function

Figure 4: *Stages 2 and 3 of our method. The user customizes the visualization of a simulation time step for highlighting the 373 Kelvin iso-therm (a) using customized iso-contours (b). The user then adds two ranges of cell death probability (c) as second variable to the transfer function (d). As expected, in the current time step, areas close to high temperatures are likely to die (hatched rim in (d)). However, the user also detects disconnected islands of high coagulation likelihood (c, top right) in proximity, possibly resulting from a previous time step. Please not that, in this case, the simulation domain extends beyond the liver wall.*

insufficient for analyzing the potential reasons for failure. In the final stage, we add a second scalar field from the simulation for concurrent analysis of both variables and their mutual interaction. We introduce textural elements to achieve a categorization of the second input variable into multiple ranges.

4.1. Stage One: Distance Evaluation

We try to visualize where a sufficient thickness of the safety margin between tumor and coagulated region border exists. We directly adopt this metaphor for visualization and attach a thick rim to the outline of the simulation. A direct visualization of the safety margin would overlay the entire ablation zone and cover a significant amount of information. To avoid this occlusion, while still communicating information about the relative width of the safety margin, we scale the rim proportionately to the 3D distance between tumor and predicted coagulation.

The IR usually prefer scrolling through the slice stack with the best resolution (*e.g.*, axial reconstruction for abdominal CT) for analysis. However, slices of the image can only convey the 2D proximity of the outlines. The actual 3D distance between simulation and tumor can drastically differ from the representation on 2D slices. Hence, we encode the 3D distance into the color of the 2D rim.

Inspecting details requires zooming in closely. Despite scaling, magnification still potentially leads to large overlays. We employ a LOD approach to further unveil data as needed. For the overview representation, we compute the thickness of the rim from the scale factor of the current slice viewer. Hence, not all views necessarily render the same LOD.

For easy reference to the outline of the coagulation zone, we additionally impose a gradient on both representations, where the white border depicts the original outline. Especially for changing signs, *i.e.*, when the outlines of tumor and coagulation zone cross, this improves readability of our technique.

LOD 1: Continuous Rim We visualize the 3D distance by encoding it in the rim width and also color-code multiple independent, customizable ranges. For example, the user might be interested in the range where the distance is definitely too small, but at the same time request a different representation for the range close to the required margin (see Figure 3(a)). Therefore, the user can setup single ranges, but also individually toggle whether they are displayed (Figure 3(c)). Zooming in also magnifies the representation accordingly. However, beyond a certain threshold, we switch to a different technique in LOD 2 for unveiling more data.

LOD 2: Sparse Representation We aim to balance the amount of information conveyed by our technique against coverage of underlying data. Upon reaching a zoom threshold, we switch to a bar chart representation of the rim, while preserving the color-based range classification (Figure 3(a),(b)). However, further magnification of these bars can again lead to significant coverage. Hence, in LOD 2, we fix the size of the bars in screen-space to a fraction of the window size, which enables arbitrary magnification (Figure 3 (b),(d))

We carefully consider placement strategies for the bars, especially during interaction: Scrolling through slice stacks and zooming result in updated contours and potentially require redistributing the bars. As soon as the zoom threshold is passed and we switch to the bar representation, we place the glyphs equidistantly on the outline related to this specific zoom factor. We limit the gap to be at least two bar widths. While scrolling, the contour length varies little. If the variation does not require adding or removing bars, we adapt the gap width for equal distribution over the contour.

The bars represent multiple bits of information. Their direction encodes that of the shortest distance on the 2D slice, whereas their length represents the 2D distance. The color, however, still relates to the range of the associated 3D distance.

Magnification drastically effects the contour length. For circumventing severe movement artifacts, we fix the relative position of the initial bars on the outline. Zooming in closer leads to an increased distance between the bars. As soon as the gap width supports an additional bar, *i.e.*, it becomes larger than twice the minimum gap plus one bar width, we recursively insert new glyphs at the center of the gap. Thereby, the displayed information remains coherent during zoom and we can ensure representation of the information by one or more bars at all times.
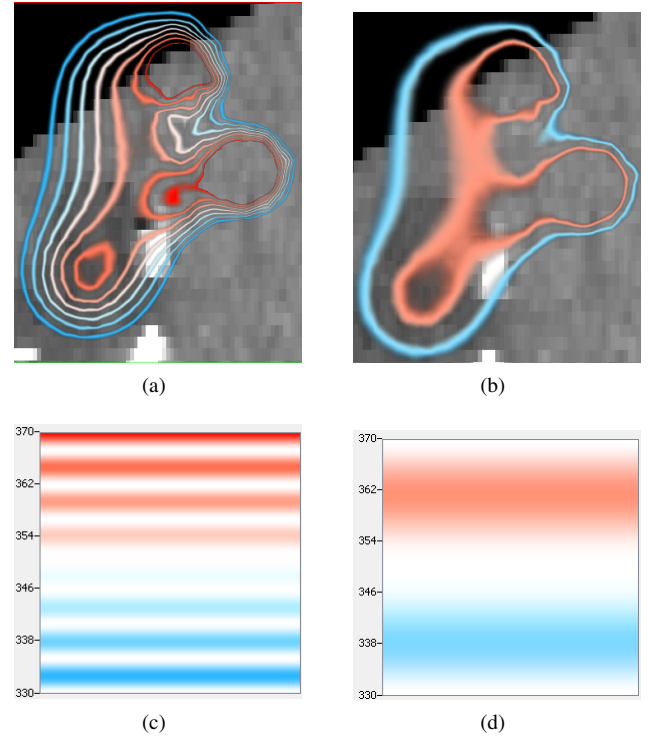
4.2. Stage 2: Scalar Field Visualization using Color

Stage 2 adds a scalar field from simulation to the distance visualization. We use color to convey the new data and provide several options for tuning the visualization. We employ an iso-contour approach, which reveals large parts of the underlying patient data, but displays sufficient information for analyzing the data field.
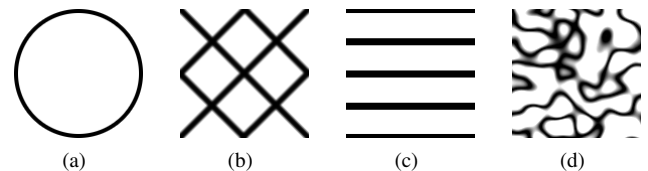
We provide several configuration possibilities. For one, the user can choose to automatically subdivide the data range into equally sized chunks. Moreover, the user can directly pick single iso-values and individually modify the widths of the contours, for which we employ a Gaussian bell-shaped opacity modulation centered at the selected iso-values. Whereas even distribution supports overview analysis, using specific contours provides a selective breakdown of the data (Figure 5). Moreover, the gradient of the scalar field around the iso-contour reflects in the width of single iso-contours (Figure 5(b)).

4.3. Stage 3: Bivariate Visualization

In the final stage, we augment the visualization with a second field from the simulation. Bivariate analysis is especially useful for evaluation of the interaction between variables. For example, a user might be interested in the overlap of regions in a certain temperature range and the corresponding cell death probability (Figure 4).

(a)   (b)

(c)   (d)

Figure 5: *The effect of the contour width parameter. If we compare the blue contours using narrow bands (a), to the wider setting (b), we deduce that the gradient in the blue area must be much higher compared to the red area. This case also reveals that a significant amount of energy, coded into the iso-contours, spreads outside the organ, which is clinically relevant.*

(a)   (b)   (c)   (d)

Figure 6: *Examples for structural textures we employ in Stage 3 for bivariate visualization. Note that these are easily extinguishable due to structure and orientation.*

We already occupy the color channel with both distance and the first scalar field, so we selected textural elements as visual variable for the final data field. Similar to the previous stage, we provide extensive control over the parameterization. The user can subdivide the data into multiple ranges and assign a textural element, which we use for drawing a textured rim at the margins of the ranges only. This avoids redundant information in large gaps between contours.

Each of the contours, which delimit the ranges, can either be an inner contour, meaning that both sides are textured, or a bounding contour, where only one side relates to a selected structure texture. Figure 4(c) shows both possibilities: The innermost iso-contour, associated with a hatched pattern, is positioned at 99% cell death

probability. For values above, the user chose no structure, so we deduct that the interior region has a cell death probability of >99%. The second displayed contour relates to both the noise pattern, as well as the hatches, easily identified as the 50% threshold from the transfer function.

We also scale the width of the rim up to a certain zoom factor. After surpassing this threshold, we switch to constant screen-space size for optimal balance of coverage versus presented information.

However, we need to be cautious about choosing the structural elements. First, the chosen textures should be partially transparent to unveil underlying data. Furthermore, zooming requires scalability of the structural elements to retain their expressiveness in context of drawing them in a rim. Finally, the structural elements should be repeatable seamlessly.

Research on texture perception suggests particular choices for the employed textures. Orientation [LB91] and local features, so-called textons [Jul81], significantly contribute to pre-attentive texture segregation. We initially provide a few samples respecting these rules (Figure 6), but our application allows usage of arbitrary elements.

Moreover, on first glance, orienting the texture elements such that their baseline coincides with segments of iso-contours seems like the most elegant representation. However, this would also mean sacrificing orientation as a powerful visual variable. Hence, we align the structure images with the axes of the viewport.

5. Implementation

We implemented our technique as a plugin for the MITK [WVW*04] framework, since it readily provides many features we require. The actual implementation is rather straight-forward, so we will keep this section brief. Our application addresses evaluation of simulated treatment, so we induce a few assumptions. The tumor outline is a necessary input for most simulation algorithms, hence we implicitly assume that the user segmented it manually or (semi-)automatically in advance. Additionally, the simulation itself needs to be present in a multi-variate representation. MICT simulation applications exploiting our evaluation techniques should provide simple means for adjusting parameters in a feedback loop for prospective optimization of treatment.

5.1. Distance Visualization

We initially compute a 3D distance field for the tumor. This is a rather time-consuming task, but only needs to be executed once per tumor and can be re-used for multiple simulation or treatment cycles. The visualization algorithm itself is implemented in OpenGL. In the first step, we compute the overall length of the coagulation zone contour visible in each frame. Additionally, we subdivide long segments. This alleviates possible issues with distance interpolation between the end points of the vertices. We then store the segments along with distance information and relative contour offsets on the GPU.

Depending on the zoom factor of a render window, we next determine the appropriate LOD. For drawing both contour and bar representation, we exploit geometry shaders. The contour method generates quads based on the respective segment and distance information. In LOD 2, we determine the bar positions based on the contour offset and the number of bars which fit within the segment. If a bar extends over the end of a segment, we automatically cut off the surplus part and delegate its rendering to the next segment. We render this stage using Multisampling Antialiasing (MSAA) for crisp outlines.

5.2. Bivariate Simulation Visualization

This technique employs a triple-pass rendering pipeline. For setup, we exploit a transfer function designer, based on a Qt interface. The result is a 2D texture, where the y-axis is responsible for visualization of the first variable, and the x-axis for the second, respectively. This, however, is only a preview for the user.

In the first rendering pass, we extract the color distribution along the y-axis for texture-based lookup during rendering the first variable. In the next pass, responsible for the second simulation field, we store the category borders selected by the user and the corresponding texture elements. We then extract iso-contours of the simulation data according to these borders and determine which texture needs to be applied to either side of the contour. We again use a geometry shader for attaching textured quads to the iso-contours. In the final stage, we again perform MSAA and blend the two previous stages using the Porter-Duff 'over' operator.

6. Evaluation

We conducted a user study to get an idea about errors in manual distance measurements during MICT as well as initial feedback about the effectiveness of our techniques for visualizing important parameters of MICT. We recruited nine medical experts (aged 28 to 40, all male) with up to six years of experience with MICT and four to twelve years of experience with slice-based visualization techniques. While one expert is currently only involved with general MICT research, the others are actively involved in up to ten MICT per month.

6.1. Procedure

After an initial discussion about MICT, we presented the experts with our bivariate visualization of simulation data in two MICT simulation data sets and gave the opportunity to explore the dataset and try to interpret the presented data using our visualization technique. To gather initial feedback about our technique, we encouraged the participants to voice their thoughts and steps they were taking. After this session, we conducted a structured interview and recorded their feedback.

In the second step of the experiment, we presented the participants with two MICT simulation datasets for comparing two techniques in a within-subject study. They were instructed to use our visual techniques as guidance for distance measurement (ours) and a traditional slice based visualization system with standard tools for in-slice distance measurement (traditional). All participants indicated that this system is equal or very similar to the tools they use in clinical practice. We randomized the order in which the techniques were presented to the participants as well as the dataset to technique

assignment. To avoid learning effects due to the within-subjects design, we chose coagulation regions with clearly different shapes. To obtain an equal number of critical regions with similar distances in both cases, we slightly modified the tumor shapes and carefully picked the target slices for measurement, which were equal in both cases.
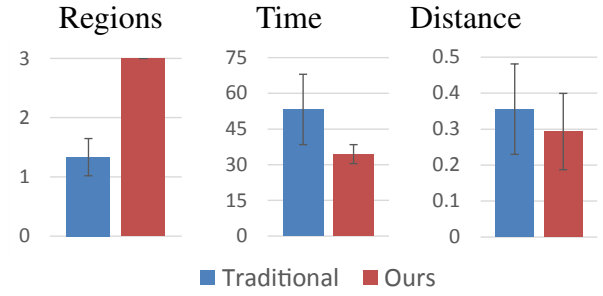
The participants had to carry out a sequence of tasks for each technique. First, we asked the participants to identify regions which show a critical distance to the tumor, *i.e.*, regions with distance smaller than 5*mm*, mark them in the slice, and measure the distance. There were no regions with negative distance, *i.e.*, failure, in the dataset. In all presented slices, there were three critical regions with a minimal distance between 3.5 and 4.8*mm*. We recorded the number of regions they found (regions) and the time it took them to find those regions (time). After they were certain that there were no more critical regions in the data, we asked the participants to measure the minimum distance of a predefined region to judge their ability to correctly measure distances with the standard measurement tools. For our approach, we disabled the distance value overlay (displaying the numerical distance value when hovering) to judge if our visualizations helps in identifying the direction required for measurement. We recorded the measured distance and computed the absolute distance to the ground-truth (distance). After completing the task sequence with each technique, we presented them with a questionnaire inquiring about their confidence of completing the task successfully. They had to answer 11 questions on a 6-point Likert-scale.

In the third step of the experiment, we revealed the full functionality (including automatic distance measurements) of the distance-based visualization technique, allowing them to evaluate their own measurement against the automatically measured data. In addition to the previous visualization, the technique now computed the closest point on the coagulated area from the current cursor position and measured the distance from this point to the tumor. We displayed this distance next to the cursor. To gain feedback about that step, we conducted a final structured interview.
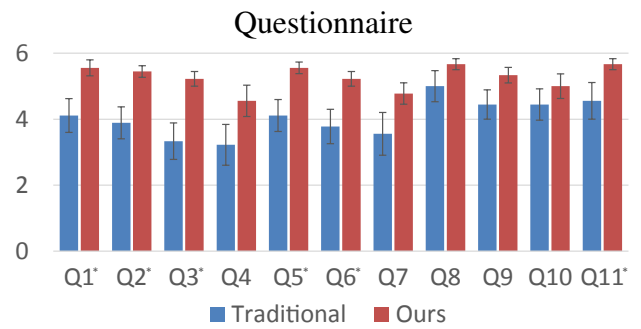
6.2. Results and Discussion

During the first part of the experiment, the medical doctors confirmed that the generation of style transfer functions with our editor is easy to learn by observing the effects of parameters. They also stated that they would probably put in effort for creating a visualization for a group of use cases once, and re-use the saved style transfer function for future cases. They mentioned that it was easy to interpret the additionally displayed data and that it would be useful to judge the details of the underlying simulation data. However, they argued that they would probably either require more training with correct interpretation of some non-obvious simulation scalar fields, *e.g.*, heat source terms or specific heat capacity, or direct assistance of an expert in biomechanical engineering. The doctors appreciated the sparse representation techniques, as they allowed them to see more of the patient data on demand.

The results of the second step of the experiment are shown in Figure 7 and Figure 8. As the measurement data was in general not normal distributed as confirmed by Shapiro-Wilk tests, we analyzed

Figure 7: *Measurement results for the traditional and ours with standard error: average number of found critial regions (out of 3); average task completion time (in seconds); average absolute distance measurement error (in mm).*

Q1 I could identify critical regions quickly
Q2 I could identify critical regions with high accuracy
Q3 I could identify critical regions with little effort
Q4 I did not miss any critical regions
Q5 I could evaluate distances within the regions with high accuracy
Q6 I could evaluate distances within the regions quickly
Q7 I could evaluate distances within the regions effortlessly
Q8 It was easy to identify tumor and coagulation boundaries
Q9 The overall mental effort was low
Q10 The visual clutter was low
Q11 I would use the method in practice

Figure 8: *Questionnaire results for the traditional technique and ours on a 6 point Likert-scale with standard error. Higher is always better (∗ means significant difference). The term critical region refers to regions which are violating the safety margin.*

all results using Friedman non-parametric tests. The measurement results for number of found regions ($\chi^2(2) = 8.0$, $p < .01$) and time ($\chi^2(2) = 5.4$, $p < .02$) showed significant effects. The difference in measured distances was not significant ($\chi^2(2) = 0.1$, $p > .70$). In the questionnaires, our method was rated higher on average for all questions. These differences were significant for Q1 ($\chi^2(2) = 6.0$, $p < .02$), Q2 ($\chi^2(2) = 4.5$, $p < .04$), Q3 ($\chi^2(2) = 4.5$, $p < .04$), Q5 ($\chi^2(2) = 6.0$, $p < .02$), Q6 ($\chi^2(2) = 6.0$, $p < .02$), and Q11 ($\chi^2(2) = 5.0$, $p < .03$). The differences were not significant for Q4 ($\chi^2(2) = 2.8$, $p > .09$), Q7 ($\chi^2(2) = 2.7$, $p > .10$), Q8 ($\chi^2(2) = 1.8$, $p > .17$), Q9 ($\chi^2(2) = 2.0$, $p > .15$), and Q10 ($\chi^2(2) = 0.2$, $p > .65$).

When using the traditional approach, only one out of the nine medical experts found all three critical regions (which took the participant 183 seconds). Two of them did not identify a single region of the three, although one participant searched for 90 seconds. When using our visualization technique, all participants found all three regions. In general, the time spent on finding and bounding the critical regions ranged from 35 to 183 seconds with the traditional approach and 32 to 68 seconds with our approach. The time spent per found region (time/#found) ranged between 28 and 122 seconds (or not found) for the traditional and between 11 and 22 seconds with ours. These results suggest that our approach has an advantage in terms of speed and accuracy over the traditional approach. The questionnaire results and interviews point into the same direction (Q1-Q3). The doctors stated that this kind of visualization could increase their confidence when scrolling through slices quickly and, thus, they would overall spend less time on individual slices. Although Q4 was n.s., we would like to mention that 7/9 doctors rated their confidence with our method higher.

The measurement errors for traditional ranged between $0.06mm$ and $1.01mm$. Using our approach for assisting manual measurements, the error was between $0.03mm$ and $0.50mm$. The questionnaire results (Q5-Q6) show that the participants had a better subjective feeling evaluating distances when being guided by a visualization. However, the visualization alone does not overcome the problems induced by drawing lines on individual 2D slices for distance measurement. This fact is confirmed by similar distance errors in the quantitative measurements. After revealing the full technique including automated distance measurements, the participants were surprised how inaccurate their manual measurements actually were. All participants said that they would highly appreciate having this feature available in clinical practice. They also commented positively that the measurements are not only shown as a static number, but allowed them to query distances all around a coagulated area, which greatly increased their confidence into the reported values.

In the questionnaires, our approach was rated equal or higher in 89 of 99 answers. Overall, the results show that participants felt confident in finding critical regions efficiently with our approach (Q1-Q3) and that it appeared easier to evaluate distances with our approach (Q5-Q6) even when performing measurements manually. While participants felt very confident in identifying coagulation boundaries (Q8) with our approach (average score of 5.7/6), they also felt confident with the traditional approach (5/6). According to the participants, our approach does not increase mental effort or visual clutter (Q9-Q10). Finally, Q11 suggests a strong tendency towards using our technique in clinical practice as compared to the de-facto standard. Seven of the doctors commented that they only use the standard ruler method, because presently there is no alternative.

7. Discussion

Our approach offers capabilities for aiding all stages of evaluation during iterative improvement of MICT simulation configurations. Whereas previous methods tackled single issues, for instance, visualizing the distance between tumor and coagulated area with regards to respecting a safety margin or cell death probability, the high configurability of our approach for multi-variate visualization enables concurrent analysis of multiple factors. While previous methods for single tasks often incorporate static configurations, for example fixed color schemes or distance ranges, the added flexibility promotes using our application for a wider range of tasks. Although not in the scope of this paper, the proposed algorithm can be used for additional tasks related to MICT immediately. For example, the distance evaluation in Stage 1 can be applied directly for analysis of real treatment with arbitrary requirements for safety margins. Pre-interventional tracking of the tumor size after Transarterial Chemoembolization (TACE) [CSO*02], or post-interventional monitoring of the coagulation area are also possible. Stage 2 can also be applied to perfusion CT [Mil03] measurements, another critical factor determining shape and extent of the coagulated region.

We consciously decided not to smooth the simulation data before visualization. Depending on the setup of the visualization, this potentially leads to visual clutter, especially in the third stage. However, capabilities for storing effective transfer functions, which sparsely display only the most relevant information, and switching between them with a few clicks, alleviates this problem to a certain degree.

Usually, simulation algorithms produce their result in multiple time steps. While we focus on analysis of a single (usually, the final) time step, our system is inherently capable of temporal analysis as well. The user can easily scroll through the time series in case they load them into the application as time-dependent datasets, which is already supported by our implementation in MITK. Additionally, temporal analysis algorithms can produce more intricate information of the behavior of the simulation over time. For instance, integration over the temperature curve using a moving window could provide more detailed information. This, however, is part of a preprocessing step and not in the scope of this paper.

8. Conclusion

We presented a modular toolset for evaluation of simulated energy-based MICT. Using different paradigms, we aid the IR throughout all stages of this procedure. Initially, we replaced evaluation of a safety margin using manual measurement via a fully automatic visual approach. In the evaluation section, we assessed the error during manual measurement and highlighted its time-consuming nature. The results of our study point towards a strong preference of our fully automatic approach, which makes evaluation not only more accurate, but also much faster. Further, we presented two more stages concerned with parameter space exploration of simulated treatment. We described a highly configurable approach for bivariate visualization of scalar fields resulting from simulation.

During initial evaluation, the participants showed particular interest in bringing the first stage into the medical practice, whereas they still might require training in understanding the physical relationships presented in Stages 2 and 3. However, they commented that the setup of the complete visualization pipeline is comparatively easy and the customization options appropriately powerful.

We plan on making our visualization tool open source and currently discuss deploying it into a first clinical trial with our medical partners. Furthermore, we currently investigate possibilities of extending our approach into a 3D representation, which might increase general acceptance of 3D methods in the radiological practice. We

also plan to build upon the initial results of our study, running a larger formal experiment with an extended user group. Given the initial feedback of medical experts, we are confident that simple, efficient visualization techniques like ours will help to increase the success of MICT in the future.

References

[AMD*15] AUDIGIER C., MANSI T., DELINGETTE H., RAPAKA S., MIHALEF V., CARNEGIE D., BOCTOR E., CHOTI M., KAMEN A., AYACHE N., ET AL.: Efficient lattice boltzmann solver for patient-specific radiofrequency ablation of hepatic tumors. *Medical Imaging, IEEE Transactions on 34*, 7 (2015), 1576–1589. 2

[BHA14] BORSIC A., HOFFER E., ATTARDO E. A.: GPU-accelerated real time simulation of radio frequency ablation thermal dose. In *2014 40th Annual Northeast Bioengineering Conference (NEBEC)* (April 2014), pp. 1–2. 2

[BWE05] BOTCHEN R., WEISKOPF D., ERTL T.: Texture-based visualization of uncertainty in flow fields. In *Visualization, 2005. VIS 05. IEEE* (Oct 2005), pp. 647–654. 3

[CBDT11] CONINX A., BONNEAU G.-P., DROULEZ J., THIBAULT G.: Visualization of uncertain scalar data fields using color scales and perceptually adapted noise. In *Proceedings of the ACM SIGGRAPH Symposium on Applied Perception in Graphics and Visualization* (New York, NY, USA, 2011), APGV '11, ACM, pp. 59–66. 3

[CSO*02] CAMMÀ C., SCHEPIS F., ORLANDO A., ALBANESE M., SHAHIED L., TREVISANI F., ANDREONE P., CRAXÌ A., COTTONE M.: Transarterial chemoembolization for unresectable hepatocellular carcinoma: meta-analysis of randomized controlled trials 1. *Radiology 224*, 1 (2002), 47–54. 9

[DBW11] DICK C., BURGKART R., WESTERMANN R.: Distance visualization for interactive 3d implant planning. *Visualization and Computer Graphics, IEEE Transactions on 17*, 12 (Dec 2011), 2173–2182. 3

[HTER04] HEALEY C. G., TATEOSIAN L., ENNS J. T., REMPLE M.: Perceptually based brush strokes for nonphotorealistic visualization. *ACM Trans. Graph. 23*, 1 (Jan. 2004), 64–96. 4

[Jul81] JULESZ B.: Textons, the elements of texture perception, and their interactions. *Nature 290*, 5802 (1981), 91–97. 7

[KERC09] KEEFE D., EWERT M., RIBARSKY W., CHANG R.: Interactive coordinated multiple-view visualization of biomechanical motion data. *IEEE Transactions on Visualization and Computer Graphics 15*, 6 (Nov. 2009), 1383–1390. 3

[KHGR02] KNISS J., HANSEN C., GRENIER M., ROBINSON T.: Volume rendering multivariate data to visualize meteorological simulations: A case study. In *Proceedings of the Symposium on Data Visualisation 2002* (Aire-la-Ville, Switzerland, Switzerland, 2002), VISSYM '02, Eurographics Association, pp. 189–ff. 4

[KKS*12] KHLEBNIKOV R., KAINZ B., STEINBERGER M., STREIT M., SCHMALSTIEG D.: Procedural texture synthesis for zoom-independent visualization of multivariate data. *Comp. Graph. Forum 31*, 3pt4 (June 2012), 1355–1364. 3

[KW06] KINDLMANN G., WESTIN C.-F.: Diffusion tensor visualization with glyph packing. *Visualization and Computer Graphics, IEEE Transactions on 12*, 5 (2006), 1329–1336. 3

[LB91] LANDY M. S., BERGEN J. R.: Texture segregation and orientation gradient. *Vision research 31*, 4 (1991), 679–691. 7

[MGT15] MARSHALL D. F., GARDNER H. J., THOMAS B. H.: Interactive visualisation for surface proximity monitoring. In *Proceedings of the 16th Australasian User Interface Conference (AUIC 2015)* (2015), vol. 27, p. 30. 3

[Mil03] MILES K. A.: Perfusion CT for the assessment of tumour vascularity: which protocol? *The British Journal of Radiology 76*, 1 (2003), S36–S42. PMID: 15456712. 9

[NIT*11] NISHIKAWA H., INUZUKA T., TAKEDA H., NAKAJIMA J., SAKAMOTO A., HENMI S., MATSUDA F., ESO Y., ISHIKAWA T., SAITO S., KITA R., KIMURA T., OSAKI Y.: Percutaneous radiofrequency ablation therapy for hepatocellular carcinoma: a proposed new grading system for the ablative margin and prediction of local tumor progression and its validation. *Journal of Gastroenterology 46*, 12 (2011), 1418–1426. 2

[POP*10] PENG T., O'NEILL D., PAYNE S., BOST C., FLANAGAN R.: Mathematical modeling of directional effects of perfusion on liver tissue temperature of radio frequency ablation. In *Proc. World Congress of Biomechanics* (2010), vol. 31. 2

[PTSP02] PREIM B., TIETJEN C., SPINDLER W., PEITGEN H.-O.: Integration of measurement tools in medical 3D visualizations. In *Visualization, 2002. VIS 2002. IEEE* (Nov 2002), pp. 21–28. 3

[RKSH11] RIEDER C., KRÖGER T., SCHUMANN C., HAHN H. K.: GPU-Based Real-Time Approximation of the Ablation Zone for Radiofrequency Ablation. *IEEE Transactions on Visualization and Computer Graphics (Proceedings Visualization 2011) 17*, 12 (December 2011), 1812–1821. 2

[Rob07] ROBERTS J. C.: State of the art: Coordinated & multiple views in exploratory visualization. In *Proceedings of the Fifth International Conference on Coordinated and Multiple Views in Exploratory Visualization* (Washington, DC, USA, 2007), CMV '07, IEEE Computer Society, pp. 61–71. 3

[ROP11] ROPINSKI T., OELTZE S., PREIM B.: Survey of glyph-based visualization techniques for spatial multivariate medical data. *Computers & Graphics 35*, 2 (2011), 392 – 401. Virtual Reality in Brazil Visual Computing in Biology and Medicine Semantic 3D media and content Cultural Heritage. 3

[RSBB06] REITINGER B., SCHMALSTIEG D., BORNIK A., BEICHEL R.: Spatial analysis tools for virtual reality-based surgical planning. In *3D User Interfaces, 2006. 3DUI 2006. IEEE Symposium on* (March 2006), pp. 37–44. 3

[RSW*09] RIEDER C., SCHWIER M., WEIHUSEN A., ZIDOWITZ S., PEITGEN H.-O.: Visualization of risk structures for interactive planning of image guided radiofrequency ablation of liver tumors, 2009. 2

[RWS*10] RIEDER C., WEIHUSEN A., SCHUMANN C., ZIDOWITZ S., PEITGEN H.-O.: Visual support for interactive post-interventional assessment of radiofrequency ablation therapy. *Computer Graphics Forum 29*, 3 (2010), 1093–1102. 2

[SI05] SHENAS H. H., INTERRANTE V.: Compositing color with texture for multi-variate visualization. In *Proceedings of the 3rd International Conference on Computer Graphics and Interactive Techniques in Australasia and South East Asia* (New York, NY, USA, 2005), GRAPHITE '05, ACM, pp. 443–446. 4

[UIM*03] URNESS T., INTERRANTE V., MARUSIC I., LONGMIRE E., GANAPATHISUBRAMANI B.: Effectively visualizing multi-valued flow data using color and texture. In *Visualization, 2003. VIS 2003. IEEE* (Oct 2003), pp. 115–121. 4

[War02] WARD M. O.: A taxonomy of glyph placement strategies for multidimensional data visualization. *Information Visualization 1*, 3/4 (Dec. 2002), 194–210. 3

[WFK*02] WONG P. C., FOOTE H., KAO D. L., LEUNG R., THOMAS J.: Multivariate visualization with data fusion. *Information Visualization 1*, 3/4 (Dec. 2002), 182–193. 4

[WVW*04] WOLF I., VETTER M., WEGNER I., NOLDEN M., BOTTGER T., HASTENTEUFEL M., SCHOBINGER M., KUNERT T., MEINZER H.-P.: The medical imaging interaction toolkit (MITK): a toolkit facilitating the creation of interactive software by extending VTK and ITK. In *Medical Imaging* (2004), pp. 16–27. 7